Structure function scaling in a $Re_\lambda = 250$ turbulent mixing layer

2011 J. Phys.: Conf. Ser. 318 042001

(http://iopscience.iop.org/1742-6596/318/4/042001)

Journal of Physics: Conference Series **318** (2011) 042001 doi:10.1088/1742-6596/318/4/042001

Structure function scaling in a $\mathrm{Re}_\lambda = 250$ turbulent mixing layer

Antonio Attili and Fabrizio Bisetti

King Abdullah University of Science and Technology
Kingdom of Saudi Arabia

E-mail: antonio.attili@kaust.edu.sa

Abstract. A highly resolved Direct Numerical Simulation of a spatially developing turbulent mixing layer is presented. In the fully developed region, the flow achieves a turbulent Reynolds number $\mathrm{Re}_\lambda = 250$, high enough for a clear separation between large and dissipative scales, so for the presence of an inertial range. Structure functions have been calculated in the self-similar region using velocity time series and Taylor's frozen turbulence hypothesis. The Extended Self-Similarity (ESS) concept has been employed to evaluate relative scaling exponents. A wide range of scales with scaling exponents and intermittency levels equal to homogeneous isotropic turbulence has been identified. Moreover an additional scaling range exists for larger scales; it is characterized by smaller exponents, similar to the values reported in the literature for flows with strong shear.

1. Introduction

There have been several investigations, experimental and numerical, to study the characteristics of turbulence and mixing of the flow downstream of the Kelvin-Helmholtz instability generated in a mixing layer. In their seminal work, Brown & Roshko (1974) analyzed the mixing layer instability and transition, emphasizing the role of coherent structures; Bell & Mehta (1990) studied the transitional mixing layer and measured turbulent statistics in the self-similar region. Measurements in different configurations have been performed by Dimotakis and coworkers (Dimotakis, 2000; Koochesfahani & Dimotakis, 1986; Dimotakis, 1991; Dimotakis & Brown, 1976). In order to characterize the differences in transitional and self-similar mixing layers and analyze inlet condition dependencies, passive and reactive scalar transport in the mixing layer has been extensively studied by Konrad (1977), Koochesfahani & Dimotakis (1986), Masutani & Bowman (1986), Clemens & Mungal (1995), Karasso & Mungal (1996). Rogers and Moser performed several direct numerical simulations; they reported a detailed analysis of the formation and dynamics of coherent large structures (Rogers & Moser, 1992; Moser & Rogers, 1991, 1993) and a description of the self-similar state (Rogers & Moser, 1994). Sandham & Sandberg (2009) analyzed the early evolution of the mixing layer originated from a splitter plate and the Brown-Roshko structures originating from the turbulent boundary layer structures upstream of the tip of the splitter plate. Laizet *et al.* (2010) performed a direct simulation to study the effect of the shape of a thick splitter plate on the mixing layer dynamics. Regardless of the large scale features of the flow, it is of great interest the statistical analysis of the turbulence generated after the transition, in particular for what concern the characteristics of the small scales and the

recovery of the universal behavior of homogeneous isotropic turbulence. One of the few studies devoted to analyze small scales turbulence in a mixing layer has been published by Wang *et al.* (2007). They performed a DNS of a spatially developing mixing layer in order to investigate the characteristics of fine scale eddies and analyze the tube-like structure already observed in homogeneous isotropic turbulence (She *et al.*, 1990; Vincent & Meneguzzi, 1991). The scaling properties for the mixing layer turbulence have been analyzed experimentally by Jiang *et al.* (2006). They described in detail longitudinal and transverse structure functions underlying the differences between scaling exponents. The general trend is a smaller value of the scaling exponents for the transverse structure functions with respect to the longitudinal ones. Moreover, for what concern the longitudinal structure functions, the main conclusion is that the scaling exponents are the same of the homogeneous isotropic turbulence.

In the present paper a highly resolved Direct Numerical Simulation (DNS) of a spatially developing turbulent mixing layer is presented. In the fully developed region, the flow achieves a turbulent Reynolds number $\mathrm{Re}_\lambda = 250$. To the authors' knowledge, the present simulation achieves the highest Reynolds number ever reported for this flow.

2. Numerical setting

The incompressible Navier-Stokes equations are solved on a structured staggered grid with a semi-implicit fractional-step method (Kim & Moin, 1985; Desjardins *et al.*, 2008). The code is implemented in parallel using the Message Passing Interface (MPI); simulations were performed on "Shaheen", an IBM Blue Gene/P supercomputer, available at King Abdullah University of Science and Technology, using up to 65536 processing cores. The boundary conditions are imposed inflow and free convective outflow (Ol'Shanskii & Staroverov, 2000) in the streamwise direction x, periodic in the spanwise direction z and free slip in the cross stream direction y; several tests have been performed to assess the effect of a finite domain in the y direction, observing negligible differences varying the length of the domain L_y, provided that L_y is large enough. The turbulent flow originates from the instability generated in the interaction of two streams with different velocities u_1 and u_2. More precisely, the condition at the inlet is a hyperbolic tangent profile with vorticity thickness $\delta_{\omega,0}$:

$$u(y)_{x=0} = U_c + \frac{1}{2}\Delta U \tanh\left(\frac{2y}{\delta_{\omega,0}}\right) \tag{1}$$

where $U_c = (u_1 + u_2)/2$ is the convective velocity and $\Delta U = u_1 - u_2$ is the velocity difference. The computational domain, spanning the region $473\delta_{\omega,0} \times 290\delta_{\omega,0} \times 157.5\delta_{\omega,0}$ ($L_x \times L_y \times L_z$), is discretized with $3072 \times 940 \times 1024 \sim 3$ billion ($n_x \times n_y \times n_z$) grid points. The domain length in the z direction is very large in order to obtain turbulence statistics independent of L_z. The resolution is enough to resolve small scales; $\delta_x < 2.5\eta$ everywhere in the domain, being $\eta = \nu^{3/4} \langle\epsilon\rangle^{-1/4}$ the Kolmogorov scale, ν and ϵ viscosity and dissipation. The $\langle . \rangle$ symbol stands for average on time and z direction. The Kelvin-Helmholtz instability is generated from the hyperbolic tangent profile imposed at the inlet, perturbed with low amplitude white noise in a layer of width $4\delta_{\omega,0}$ around $y = 0$.

3. Streamwise evolution of turbulence statistics

Figures 1 and 2 show the streamwise evolution of mean and fluctuations profiles for the streamwise components of velocity, for several downstream locations. Table 1 contains a list of the x coordinates of all the locations reported in the graphs. In the streamwise evolution the mean width increases and the momentum thickness is typically used to describe the local size

Table 1. Stremwise locations reported in the graphs

	A	B	C	D	E	F	G	H	I	L
Streamwise location $(x/\delta_{\omega,0})$	0	50	100	150	200	250	300	350	400	450

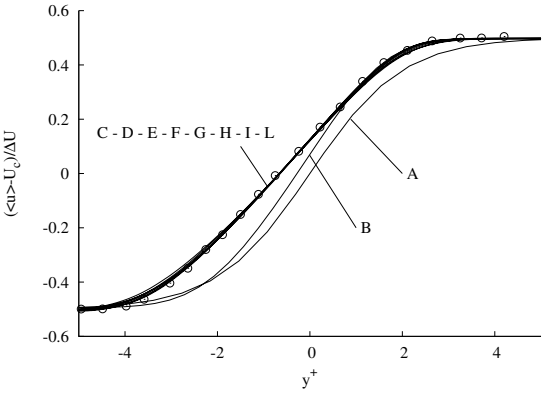

Figure 1. Mean velocity profiles for several downstream locations (solid lines). Circles: measurements from Bell & Mehta (1990). The y coordinate is scaled with the local momentum thickness.

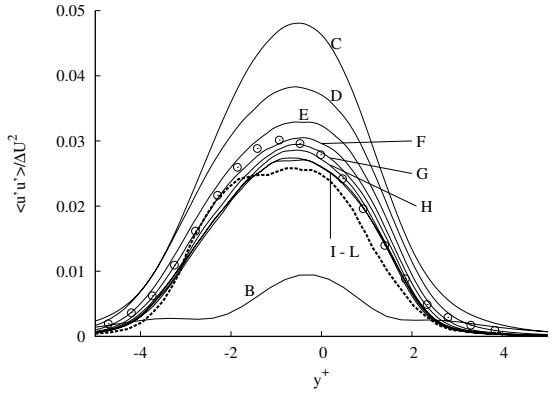

Figure 2. Variance of the streamwise velocity component for several downstream locations (solid lines). Dashed line: DNS from Rogers & Moser (1994). Circles: experimental measurements from Bell & Mehta (1990).

of the layer:

$$\delta_\theta(x) = \int_{-\infty}^{\infty} (u_1 - \langle u \rangle)\,(\langle u \rangle - u_2)\,dy \tag{2}$$

In all the graphs the cross-stream spatial coordinate has been scaled with the local momentum thickness: $y^+ = y/\delta_\theta(x)$. Convergence to an approximate self-similarity behavior can be observed for the profiles. Also included are the results from the DNS by Rogers & Moser (1994) of a temporal evolving mixing layer with turbulent initial conditions and the experiments by Bell & Mehta (1990) for a mixing layer begun from turbulent (tripped) splitter plate boundary layers. Self similarity implies a linear growth for total turbulent kinetic energy (Clark & Zhou, 2003):

$$K(x) = \frac{1}{2}\int_{-\infty}^{\infty} \langle u'u' \rangle + \langle v'v' \rangle + \langle w'w' \rangle\,dy \sim x \tag{3}$$

Figure 3 shows that the total turbulent kinetic energy, after the Kelvin-Helmholtz instability, grows linearly. The three components of the kinetics energy are also reported; the total $\langle u'u' \rangle$ achieves the linear growth behavior before the other two components, that overshoot the linear behavior in the region where strong vortex pairings occur (Moser & Rogers, 1993).

4. Structure functions

Statistical properties of turbulence in the inertial range can be characterized in terms of longitudinal velocity structure functions (Monin & Yaglom, 1971; Frisch, 1995). The nth-order longitudinal structure function, for the streamwise component of velocity, is defined, at the **x**

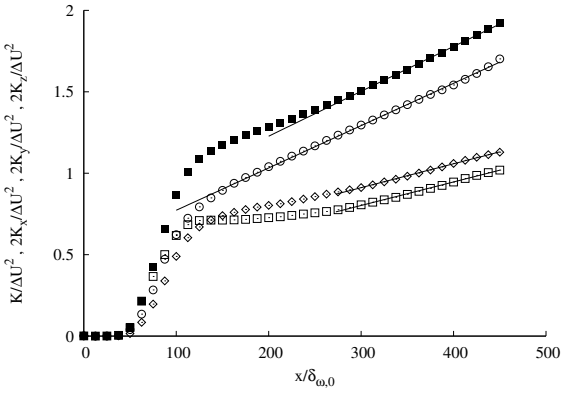

Figure 3. Streamwise evolution of total turbulent kinetic energy (filled symbols). The three components are also shown separately (open symbols). Circle: $2K_x = \int_{-\infty}^{\infty} \langle u'u' \rangle \, dy$. Squares: $2K_y = \int_{-\infty}^{\infty} \langle v'v' \rangle \, dy$. Diamonds: $2K_z = \int_{-\infty}^{\infty} \langle w'w' \rangle \, dy$. Lines are least squares fits in the ranges $200 < x/\delta_{\omega,0} < 400$ for K_x and $300 < x/\delta_{\omega,0} < 400$ for K, K_y and K_z.

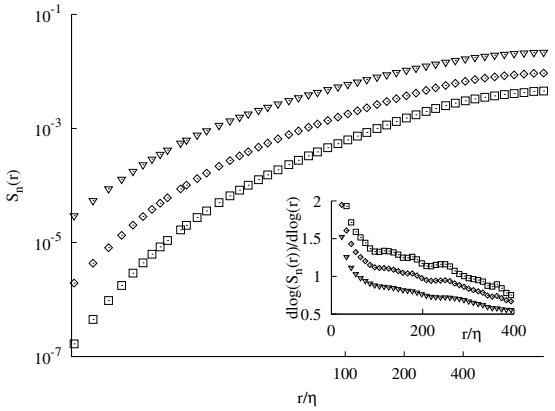

Figure 4. 3rd (triangles), 4th (diamonds) and 5th-order (squares) structure functions. Inset: local slope $\mathrm{d}\log S_n/\mathrm{d}\log r$ for the same structure functions.

position, as:

$$S_n(\mathbf{x}, r) = \langle |u(\mathbf{x}+r) - u(\mathbf{x})|^n \rangle. \tag{4}$$

where r (separation) is a distance in the streamwise direction. Theoretical, experimental and numerical studies support the idea that S_n has a universal power-law dependence on r in the inertial range: $S_n(r) \sim r^{\zeta(n)}$. Universality refers to the scaling exponents being independent of the mean of turbulence generation. A fundamental result established by a number of studies (see Frisch (1995) for a detailed review) is that the values of the exponents differ from those implied by Kolmogorov's 1941 theory (Kolmogorov, 1941*c*,*b*,*a*) (henceforth referred to as K41), i.e. $\zeta(n) = n/3$; moreover the exponents are universal in the homogeneous isotropic limit. The longitudinal velocity structure functions up to 6th-order are evaluated in the mixing layer using velocity signals sampled in time and applying Taylor's hypothesis. For what concern the scaling of structure functions, time signals instead of spatial flow fields have been widely used in experimental works (Anselmet *et al.*, 1984; Jiang *et al.*, 2006; Arneodo *et al.*, 1996; Benzi *et al.*, 1995), where measuring spatial evolutions is extremely difficult; comparing the cited results obtained using time signals with other results obtained using numerical simulations and analysing spatial data (Watanabe & Gotoh, 2004), it can be observed that the conclusions established applying the Taylor hypothesis are equivalent to results obtained with the analysis of the spatial structures of the flow field. A detailed analysis of the applicability of the Taylor's hypothesis in the contest of structure functions scaling is reported by Lvov *et al.* (1999). For the ranges of parameters in our configuration it is possible to estimate a systematic error of the order of 0.01 for the 2nd order structure function exponent, related to the use of the temporal surrogates of the spatial statistics. This error does not affect the conclusions of the present analysis. The velocity probes are located in a region of fully developed turbulence at $x = 400\delta_{\omega,0}$ and $y = -4\delta_{\omega,0}$. The crosswise coordinate was selected to coincide with the location of maximum turbulent kinetic energy at the given streamwise location. Figure 4 shows the 3rd, 4th and 5th-order structure functions recovered from the DNS data. It is not possible to identify a scaling range because the Reynolds number is not large enough. In order to understand how far from the

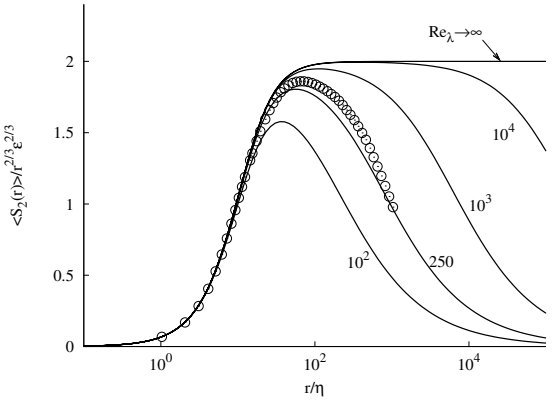

Figure 5. Comparison of the second order structure function (circles) with the model in eq. 5 for isotropic turbulence (solid lines); the model equation is plotted for several values of Re_λ.

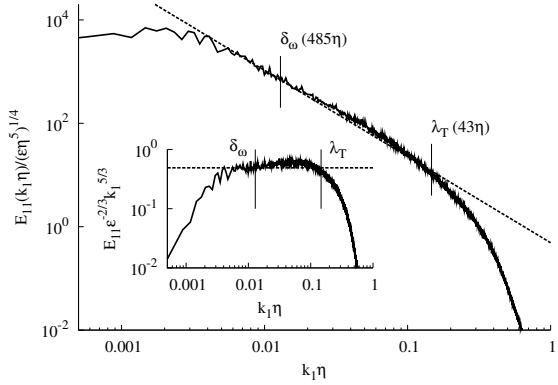

Figure 6. Longitudinal one-dimensional energy spectrum of the streamwise velocity component, normalized by the Kolmogorov units. The inset shows the compensated spectrum, $E_{11}\epsilon^{-2/3}k_1^{5/3}$. Dashed lines are the universal spectra with $-5/3$ power law and $18/55C_k$ intercept, ($C_k = 1.5$ is the Kolmogorov constant). The vertical solid lines mark the wavelengths corresponding to Taylor microscale ($\lambda_T \approx 43\eta$) and local vorticity thickness of the layer ($\delta_\omega \approx 485\eta$).

infinite Reynolds number limit the present configuration is, we compared the 2nd order structure function calculated from the DNS with a model that takes into account finite Reynolds numbers effects. Recently Antonia & Burattini (2006) analyzed Reynolds number (Re_λ) effects on the 2nd and 3rd order structure functions for grid turbulence (with energy decay in the streamwise direction) and a forced periodic box. They used the following description for the 2nd order structure function as a function of R_λ (see also Antonia *et al.* (2003) and Kurien & Sreenivasan (2000)):

$$S_2(r^*) = \frac{r^{*2}}{15}\frac{(1+\beta r^*)^{2c-2}}{(1+(r^*/r^*_{cu})^2)^c} \tag{5}$$

The $*$ indicates non-dimensionalization with the Kolmogorov scale η, r^*_{cu} is the crossover between dissipative and inertial ranges, $c = (1-\zeta(2)/2)$ and $\beta = L^{*-1}$, with L the integral lenghtscale. Equation 5 is a modification, for finite Reynolds number, of the model proposed by Batchelor (1951). For isotropic turbulence, the non-dimensional Taylor scale is $\lambda^* = 15^{1/4}\mathrm{Re}_\lambda^{1/2}$, $\langle u'^* u'^* \rangle = \mathrm{Re}_\lambda/15^{1/2}$ and $L^* = 15^{-3/4}C_\epsilon \mathrm{Re}_\lambda^{3/2}$ with $L = C_\epsilon \langle u'u' \rangle^{3/2} / \langle \epsilon \rangle$. A value of 1 for the dimensionless energy dissipation $C\epsilon$ is assumed and $r^*_{cu} = (15C_{u2})^{3/4}$ with a value of 2 for the Kolmogorov constant C_{u2}. This model can represent well the shape of the structure function and the effect of Re_λ (Antonia & Burattini, 2006; Kurien & Sreenivasan, 2000). A comparison of the second order structure function obtained from the DNS with the model in eq. 5 is reported in figure 5. The Kolmogorov theory predicts, for the compensated structure function reported in the graph, an asymptotic value of 2 ($\mathrm{Re}_\lambda \to \infty$). For our simulation the Reynolds number is around 250, not enough for the existence of an inertial range (a plateau close to the value 2). The general agreement between the data and the model is good, especially for $r/\eta < 100$, showing that the turbulence generated by the mixing layer is very similar to the homogeneous isotropic case. For larger scales the discrepancy can be related to the effects of mean shear

and coherent structures generated by the Kelvin-Helmholtz instability and the vortex pairings, typical of the shear layer configuration. Structure functions have been analyzed in a range of scales that extends from a few Kolmogorov scales up to the large scale size of the mixing layer. Characteristic scales, relevant in the analysis that follows, are marked in figure 6, that shows the longitudinal one-dimensional energy spectrum of the streamwise velocity component, normalized by the Kolmogorov units. The inertial range, with an approximate $-5/3$ scaling, is almost completely affected by the bump related to predissipative bottleneck effects (Meyers & Meneveau, 2008); this characteristics is an additional measure of the degree of convergence to the high Reynolds asymptotic behavior. In order to analyse scaling properties in the case of moderate Reynolds numbers, it is convenient to apply the Extended Self-Similarity (ESS) concept (Benzi *et al.*, 1993; Arneodo *et al.*, 1996; Segel *et al.*, 1996; Grossmann *et al.*, 1997). Instead of plotting log-log plots of $S_n(r)$ vs r, plotting log-log plots of $S_n(r)$ vs $S_2(r)$ or $S_3(r)$ reveals much longer scaling ranges that can be used to fit accurate exponents. Rather than the direct exponents $\zeta(n)$, the relative exponents $\gamma_{n,2} = \zeta(n)/\zeta(2)$ and $\gamma_{n,3} = \zeta(n)/\zeta(3)$ are computed as follows:

$$\gamma_{n,\alpha} = \frac{\zeta(n)}{\zeta(\alpha)} = \frac{\mathrm{d}\log S_n(r)}{\mathrm{d}\log S_\alpha(r)} \text{ with } \alpha = 2, 3 \tag{6}$$

where $\mathrm{d}\log S_n(r)/\mathrm{d}\log S_2(r)$ and $\mathrm{d}\log S_n(r)/\mathrm{d}\log S_3(r)$ are the relative logarithmic derivatives.

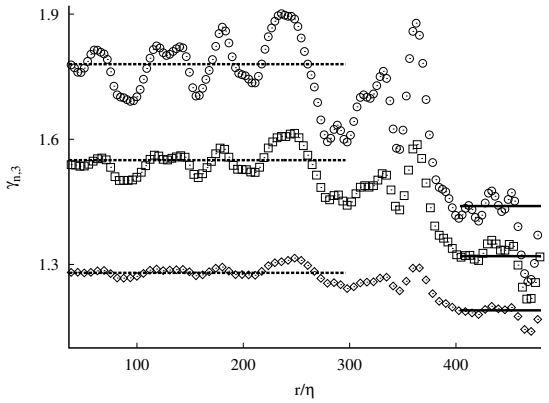

Figure 7. Relative logarithmic derivative $\mathrm{d}\log S_n(r)/\mathrm{d}\log S_3(r)$ as a function of separation r for structure functions of 4th (diamonds), 5th (squares), and 6th-order (circles). The solid lines represent the relative exponent $\gamma_{n,3}$ obtained as an average over $60 < r/\eta < 250$. The dashed lines represent the same relative exponent averaged over the range $400 < r/\eta < 460$.

Figure 7 shows the value of the relative logarithmic derivative of three structure functions ($n = 4, 5, 6$) plotted versus the normalized separation distance r/η. The value of the relative exponents $\gamma_{n,3}$ fluctuate over the whole range of separation distances considered. The fluctuations are more pronounced for higher-order structure functions (e.g. compare structure functions $n = 4$ and $n = 6$). Despite the fluctuations, it is possible to identify a wide range of scale ($60 < r/\eta < 250$) with approximately constant scaling exponents. The values of the exponents, averaged over this range, are in extremely good agreement with the case of homogeneous isotropic turbulence. In the range of scales considered, the set of exponents is independent of the flow particular geometry, the large scales features and the way turbulence have been generated; the universal behavior characteristic of isotropic turbulence is recovered. This conclusion is in agreement with the results by Jiang *et al.* (2006). They reported an experimental study of several turbulent mixing layers, up to a Reynolds number $\mathrm{Re}_\lambda = 237$, a value close to the conditions of our simulation ($\mathrm{Re}_\lambda = 250$). They focused their analysis in the range of scales $50\eta < r < 250\eta$ and found that the scaling of longitudinal structure functions is the same of homogeneous isotropic turbulence. In fig. 7, it can be also observed that, at larger scales ($400 < r/\eta < 460$), there exist an additional scaling range, characterized by a larger deviation from the K41 linear prediction. In order to better characterize this additional scaling we analyzed two observables routinely used (Ruiz-Chavarria *et al.*, 2000; Casciola *et al.*, 2001) in the context of ESS: $\sigma_n = S_n/S_2^{n/2}$

and $\rho_n = S_n/S_3^{n/3}$, which are typically plotted in logarithmic scale versus the structure function $S_2(r)$ and $S_3(r)$, respectively. Their logarithmic derivative is related to the relative exponents:

$$\frac{\mathrm{d}\log\sigma_n}{\mathrm{d}\log S_2} = \gamma_{n,2} - \frac{n}{2} \quad \text{and} \tag{7}$$

$$\frac{\mathrm{d}\log\rho_n}{\mathrm{d}\log S_3} = \gamma_{n,3} - \frac{n}{3}. \tag{8}$$

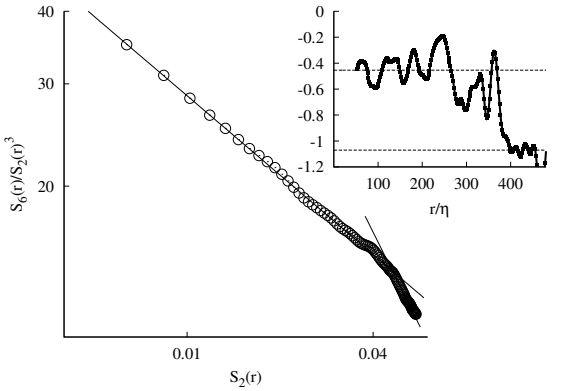

Figure 8. The observable $\sigma_6 = S_6/S_2^3$ is plotted as a function of S_2 in logarithmic scale. For $60 < r/\eta < 250$ the data are fitted by a power law with slope equal to -0.43 ($\gamma_{6,2} = 2.57$). For larger scales ($400 < r/\eta < 460$) the slope is -1.06 ($\gamma_{6,2} = 1.94$). Inset: local slope versus local separation.

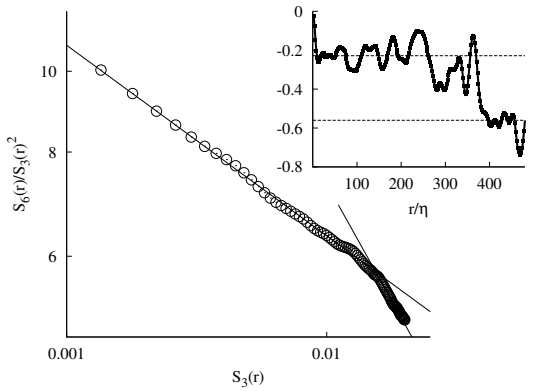

Figure 9. The observable $\rho_6 = S_6/S_3^2$ is plotted as a function of S_3 in logarithmic scale. For $60 < r/\eta < 250$ the data are fitted by a power law with slope equal to -0.22 ($\gamma_{6,3} = 1.78$). For larger scales ($400 < r/\eta < 460$) the slope is -0.56 ($\gamma_{6,3} = 1.44$). Inset: local slope versus local separation.

Figures 8 and 9 illustrate the behavior of σ_6 and ρ_6 as a function of S_2 and S_3 recovered from the DNS data. The slope of the curve in a log-log plot is equal to the deviation with respect to K41 theory, so it is a measure of intermittency. The homogeneous isotropic turbulence scaling clearly appears in the range $60 < r/\eta < 250$. For larger scales the same exponent is not applicable and a different least squares fitting (over the range of S_2 and S_3 corresponding to $400 < r/\eta < 460$) has been performed, obtaining a different exponent. The local slopes Eq. (7) and (8) are shown in the insets. The scale $r = 400\eta$ corresponds roughly to 10 shear length scales $L_S = \sqrt{\epsilon/S^3}$, S being the local mean shear. This estimation of the shear length scale is derived from dimensional analysis (so there may be a multiplicative prefactor in its expression) and under the assumption of equilibrium in the production-dissipation balance so it has to be considered an approximation in the present configuration. A similar behavior for the large scales range ($r > 10L_S$), with the same relative scaling exponents, has been observed by Ruiz-Chavarria *et al.* (2000) for a boundary layer experiment. The values of the large scales scaling exponents, obtained in the mixing layer, are also in good agreement with other studies of strong shear configurations. The relative exponents, averaged over the two ranges, are compared to those reported in several experimental and numerical studies published in the literature. Figure 10 contains a summary of these results, plotted as differences with respect to the Kolmogorov's K41 linear scaling (horizontal line). Scaling exponents for homogeneous isotropic turbulence and for several flows characterized by strong shear are reported for comparison.

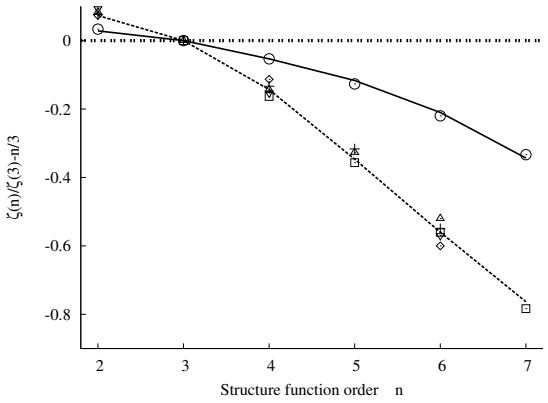

Figure 10. Summary of scaling exponents for the mixing layer; difference with respect to the Kolmogorov's K41 scaling (horizontal line). Exponents for $60\eta < r < 250\eta$ (solid line) and $400\eta < r < 460\eta$ (dashed line). Results for homogeneous turbulence (Frisch, 1995; Watanabe & Gotoh, 2004; Benzi *et al.*, 1995) (open circles) and several shear flows: near the wall in a channel numerical simulation (Toschi *et al.*, 1999; Benzi *et al.*, 1999) (⊡), in a channel experiment (Onorato *et al.*, 2000) (△), in the logarithmic sublayer of a boundary layer flow (Ruiz-Chavarria *et al.*, 2000) (+), in a wake experiment (Gaudin *et al.*, 1998) (⋄), in a Kolmogorov flow with anisotropic forcing (Benzi *et al.*, 1996) (▽).

5. Conclusions

A detailed direct numerical simulation of a turbulent, spatially developing, mixing layer has been performed. The statistical features of the turbulent field downstream of the Kelvin-Helmholtz instability has been analyzed in terms of the scaling of longitudinal velocity structure functions. Scaling exponents have been evaluated using the Extended Self-Similarity approach and compared with the values available in the literature for other flow configurations. A wide range with scaling exponents and intermittency level equal to homogeneous isotropic turbulence can be identified. Moreover, an additional scaling range appears at large scales, with exponents similar to the values reported in the literature in configurations with strong shear.

References

Anselmet, F., Gagne, Y., Hopfinger, EJ & Antonia, RA 1984 High-order velocity structure functions in turbulent shear flows. *J. Fluid Mech.* **140** (-1), 63–89.

Antonia, R.A. & Burattini, P. 2006 Approach to the 4/5 law in homogeneous isotropic turbulence. *J. Fluid Mech.* **550**, 175–184.

Antonia, R.A., Smalley, R.J., Zhou, T., Anselmet, F. & Danaila, L. 2003 Similarity of energy structure functions in decaying homogeneous isotropic turbulence. *J. Fluid Mech.* **487**, 245–269.

Arneodo, A., Baudet, C., Belin, F., Benzi, R., Castaing, B., Chabaud, B., Chavarria, R., Ciliberto, S., Camussi, R., Chilla, F. *et al.* 1996 Structure functions in turbulence, in various flow configurations, at Reynolds number between 30 and 5000, using extended self-similarity. *Europhys. Lett.* **34**, 411.

Batchelor, G.K. 1951 Pressure fluctuations in isotropic turbulence. In *MPCPC*, , vol. 47, pp. 359–374. Cambridge Univ Press.

Bell, J. & Mehta, R. 1990 Development of a two-stream mixing layer from tripped and untripped boundary layers. *AIAA J.* **28** (12), 2034–2042.

Benzi, R., Amati, G., Casciola, C.M., Toschi, F. & Piva, R. 1999 Intermittency and scaling laws for wall bounded turbulence. *Phys. Fluids* **11**, 1284.

Benzi, R., Ciliberto, S., Baudet, C. & Chavarria, G.R. 1995 On the scaling of three-dimensional homogeneous and isotropic turbulence. *Physica D* **80** (4), 385–398.

Benzi, R., Ciliberto, S., Tripiccione, R., Baudet, C., Massaioli, F. & Succi, S. 1993 Extended self-similarity in turbulent flows. *Phys. Rev. E* **48** (1), 29–32.

Benzi, R., Struglia, MV & Tripiccione, R. 1996 Extended self-similarity in numerical simulations of three-dimensional anisotropic turbulence. *Phys. Rev. E* **53** (6), 5565–5568.

Brown, G.L. & Roshko, A. 1974 On density effects and large structure in turbulent mixing layers. *J. Fluid Mech.* **64** (04), 775–816.

Casciola, C.M., Benzi, R., Gualtieri, P., Jacob, B. & Piva, R. 2001 Double scaling and intermittency in shear dominated flows. *Phys. Rev. E* **65** (1), 15301.

Clark, T.T. & Zhou, Y. 2003 Self-similarity of two flows induced by instabilities. *Phys. Rev. E* **68** (6), 66305.

Clemens, N.T. & Mungal, M.G. 1995 Large-scale structure and entrainment in the supersonic mixing layer. *J. Fluid Mech.* **284**, 171–216.

Desjardins, O., Blanquart, G., Balarac, G. & Pitsch, H. 2008 High order conservative finite difference scheme for variable density low Mach number turbulent flows. *J. Comput. Phys.* **227** (15), 7125–7159.

Dimotakis, P.E. 1991 Turbulent free shear layer mixing and combustion. *High Speed Flight Propulsion Systems* pp. 265–340.

Dimotakis, P.E. 2000 The mixing transition in turbulent flows. *J. Fluid Mech.* **409**, 69–98.

Dimotakis, P.E. & Brown, G.L. 1976 The mixing layer at high Reynolds number: large-structure dynamics and entrainment. *J. Fluid Mech.* **78** (03), 535–560.

Frisch, U. 1995 *Turbulence: the legacy of AN Kolmogorov*. Cambridge Univ Pr.

Gaudin, E., Protas, B., Goujon-Durand, S., Wojciechowski, J. & Wesfreid, JE 1998 Spatial properties of velocity structure functions in turbulent wake flows. *Phys. Rev. E* **57** (1), 9–12.

Grossmann, S., Lohse, D. & Reeh, A. 1997 Application of extended self-similarity in turbulence. *Phys. Rev. E* **56** (5), 5473.

Jiang, X.Q., Gong, H., Liu, J.K., Zhou, M.D. & She, Z.S. 2006 Hierarchical structures in a turbulent free shear flow. *J. Fluid Mech.* **569**, 259–286.

Karasso, P.S. & Mungal, M.G. 1996 Scalar mixing and reaction in plane liquid shear layers. *J. Fluid Mech.* **323**, 23–63.

Kim, J. & Moin, P. 1985 Application of a fractional-step method to incompressible Navier-Stokes equations. *J. Comput. Phys.* **59** (2), 308–323.

Kolmogorov, A.N. 1941*a* Energy dissipation in locally isotropic turbulence. *CR Acad. Sci. URSS* **32**, 16.

Kolmogorov, A.N. 1941*b* On degeneration of isotropic turbulence in an incompressible viscous liquid, CR (Doklady) Acad. *CR Acad. Sci. URSS* **31**, 538.

Kolmogorov, A.N. 1941*c* The local structure of turbulence in incompressible viscous fluid for very large Reynolds. *CR Acad. Sci. URSS* **30**, 301.

Konrad, J.H. 1977 An experimental investigation of mixing in two-dimensional turbulent shear flows with application to diffusion-limited chemical reactions. PhD thesis, California Institute of Technology.

Koochesfahani, M.M. & Dimotakis, P.E. 1986 Mixing and chemical reactions in a turbulent liquid mixing layer. *J. Fluid Mech.* **170**, 83–112.

Kurien, S. & Sreenivasan, K.R. 2000 Anisotropic scaling contributions to high-order structure functions in high-Reynolds-number turbulence. *Phys. Rev. E* **62** (2), 2206–2212.

Laizet, S., Lardeau, S. & Lamballais, E. 2010 Direct numerical simulation of a mixing layer downstream a thick splitter plate. *Phys. Fluids* **22**, 015104.

Lvov, V. S., Pomyalov, A. & Procaccia, I. 1999 Temporal surrogates of spatial turbulent statistics: The taylor hypothesis revisited. *Phys. Rev. E* **60** (4), 4175.

Masutani, S.M. & Bowman, C.T. 1986 The structure of a chemically reacting plane mixing layer. *J. Fluid Mech.* **172**, 93–126.

Meyers, J. & Meneveau, C. 2008 A functional form for the energy spectrum parametrizing bottleneck and intermittency effects. *Phys. Fluids* **20**, 065109.

Monin, A. S. & Yaglom, A. M. 1971 *Statistical Fluid Mechanics*. MIT Press, Cambridge.

Moser, R.D. & Rogers, M.M. 1991 Mixing transition and the cascade to small scales in a plane mixing layer. *Phys. Fluids* **3**, 1128.

Moser, R.D. & Rogers, M.M. 1993 The three-dimensional evolution of a plane mixing layer: pairing and transition to turbulence. *J. Fluid Mech.* **247** (-1), 275–320.

Ol'Shanskii, M.A. & Staroverov, V.M. 2000 On simulation of outflow boundary conditions in finite difference calculations for incompressible fluid. *Int. J. Numer. Methods Fluid* **33** (4), 499–534.

Onorato, M., Camussi, R. & Iuso, G. 2000 Small scale intermittency and bursting in a turbulent channel flow. *Phys. Rev. E* **61** (2), 1447–1454.

Rogers, M.M. & Moser, R.D. 1992 The three-dimensional evolution of a plane mixing layer: the Kelvin–Helmholtz rollup. *J. Fluid Mech.* **243** (-1), 183–226.

Rogers, M. M. & Moser, R. D. 1994 Direct simulation of a self-similar turbulent mixing layer. *Phys. Fluids* **6**, 903.

Ruiz-Chavarria, G., Ciliberto, S., Baudet, C. & Leveque, E. 2000 Scaling properties of the streamwise component of velocity in a turbulent boundary layer. *Physica D* **141** (3-4), 183–198.

Sandham, N.D. & Sandberg, R.D. 2009 Direct numerical simulation of the early development of a turbulent mixing layer downstream of a splitter plate. *J. Turbul.* **10** (1), 1–17.

Segel, D., L'vov, V. & Procaccia, I. 1996 Extended self-similarity in turbulent systems: an analytically soluble example. *Phys. Rev. Lett.* **76** (11), 1828–1831.

She, Z.S., Jackson, E. & Orszag, S.A. 1990 Intermittent vortex structures in homogeneous isotropic turbulence. *Nature* **344** (6263), 226–228.

Toschi, F., Amati, G., Succi, S., Benzi, R. & Piva, R. 1999 Intermittency and structure functions in channel flow turbulence. *Phys. Rev. Lett.* **82** (25), 5044–5047.

Vincent, A. & Meneguzzi, M. 1991 The spatial structure and statistical properties of homogeneous turbulence. *J. Fluid Mech.* **225**, 1–20.

Wang, Y., Tanahashi, M. & Miyauchi, T. 2007 Coherent fine scale eddies in turbulence transition of spatially-developing mixing layer. *Int. J. Heat Fluid Flow* **28** (6), 1280–1290.

Watanabe, T. & Gotoh, T. 2004 Statistics of a passive scalar in homogeneous turbulence. *New J. Phys.* **6**, 40.